Unimolecular micelles as an effective carrier of poorly water-soluble nifuratel for selective *in vivo* anticervical cancer therapy via mucoadhesive dynamic hydrogels

Monika Gosecka[1]*, Mateusz Gosecki[1], Malgorzata Urbaniak[1], Ewelina Wielgus[1], Renata Gruszka[2], Monika Marcinkowska[3], Barbara Klajnert-Maculewicz[3], Anna Janaszewska[3]*

[1] Centre of Molecular and Macromolecular Studies, Polish Academy of Sciences, Sienkiewicza 112, 90-363 Lodz, Poland
[2] Department of Molecular Biotechnology and Genetics, Faculty of Biology and Environmental Protection, University of Lodz, Banacha 12/16, 90-237 Lodz, Poland
[3] Department of General Biophysics, Faculty of Biology and Environmental Protection, University of Lodz, 141/143 Pomorska, 90-236 Lodz, Poland

Correspondence email: mdybko@cbmm.lodz.pl

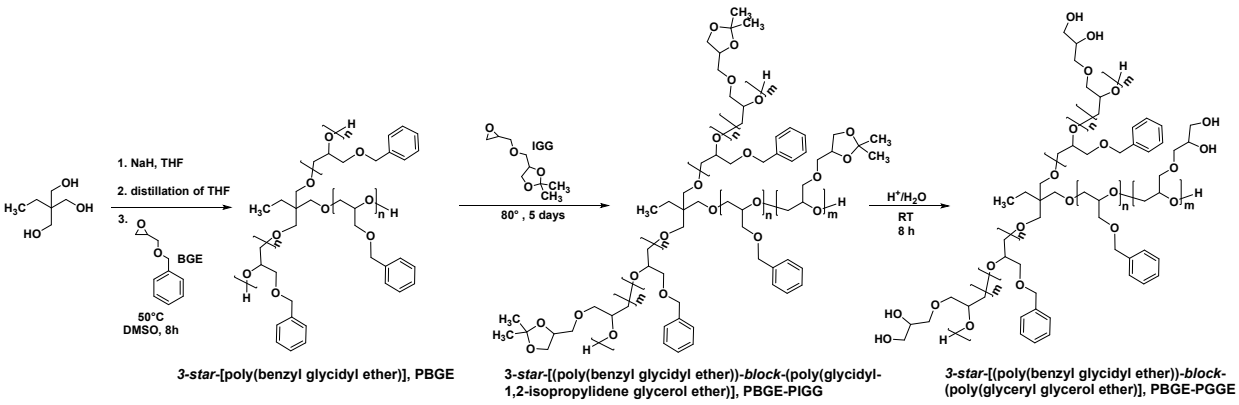

Scheme S1. Scheme showing the synthesis route of three-arm copolyethers with hydrophobic poly(benzyl glycidyl ether)-based core and hydrophilic shell based on poly(glyceryl glycerol ether).

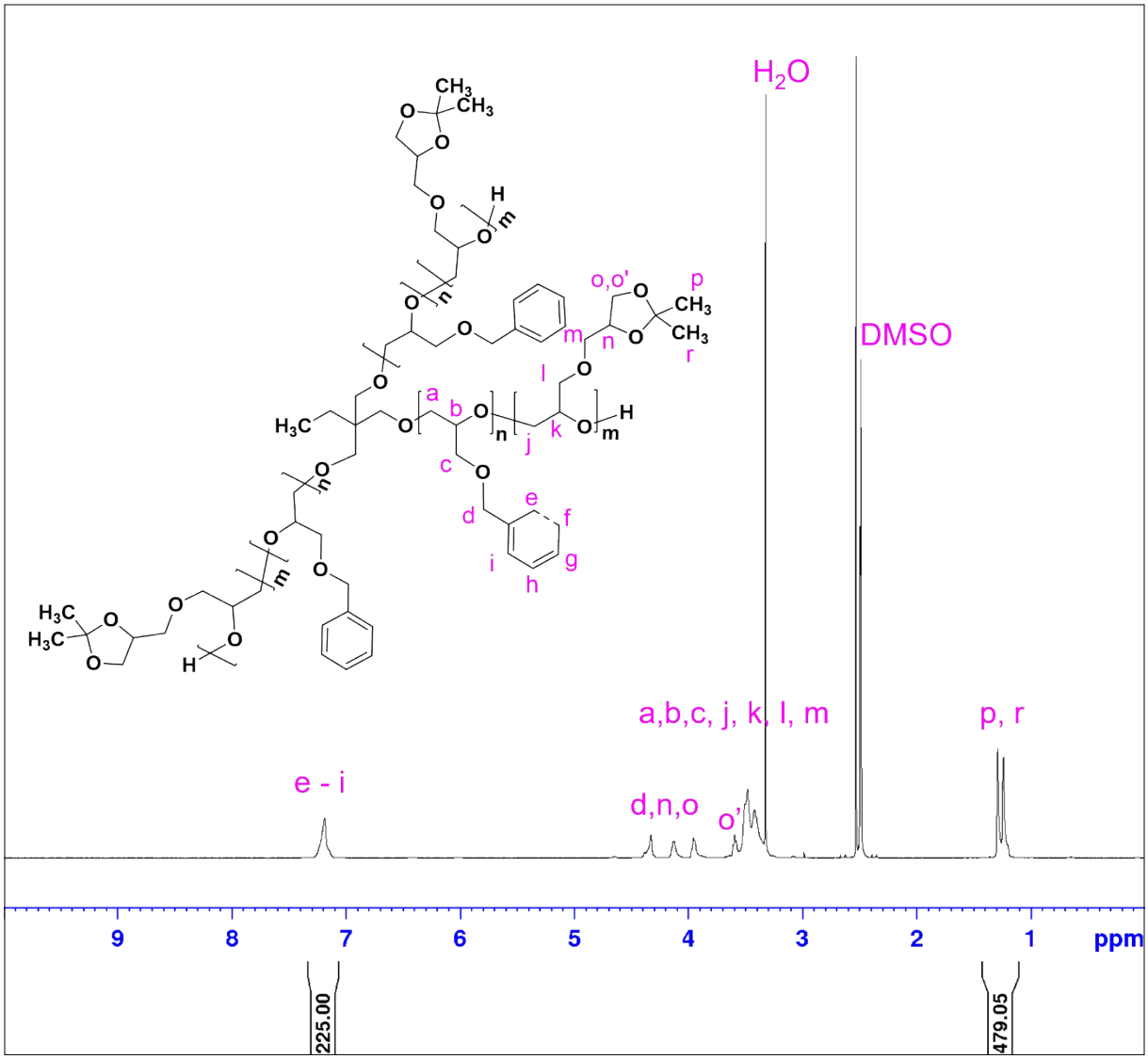

Figure S1. ^{1}H NMR spectrum of PBGE-PIGGE_1 recorded in DMSO-d_6.

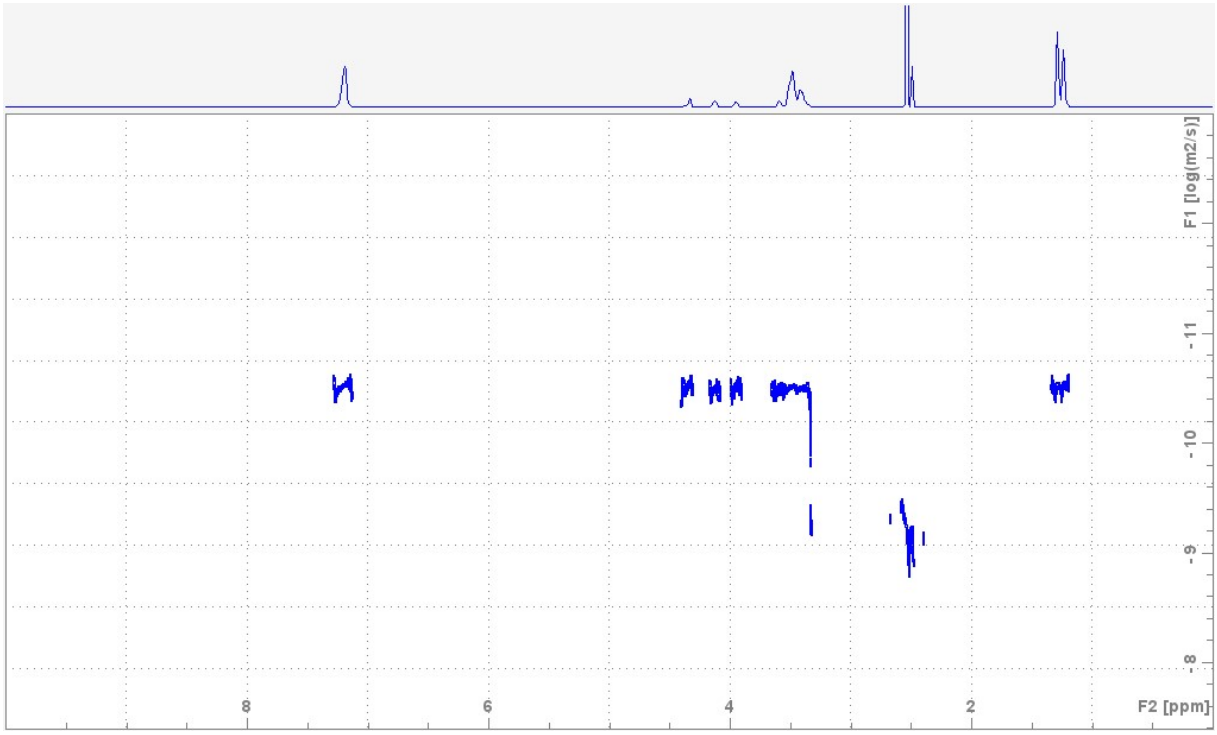

Figure S2. ^{1}H DOSY NMR spectrum of PBGE-PIGGE_1 recorded in DMSO-d_6.

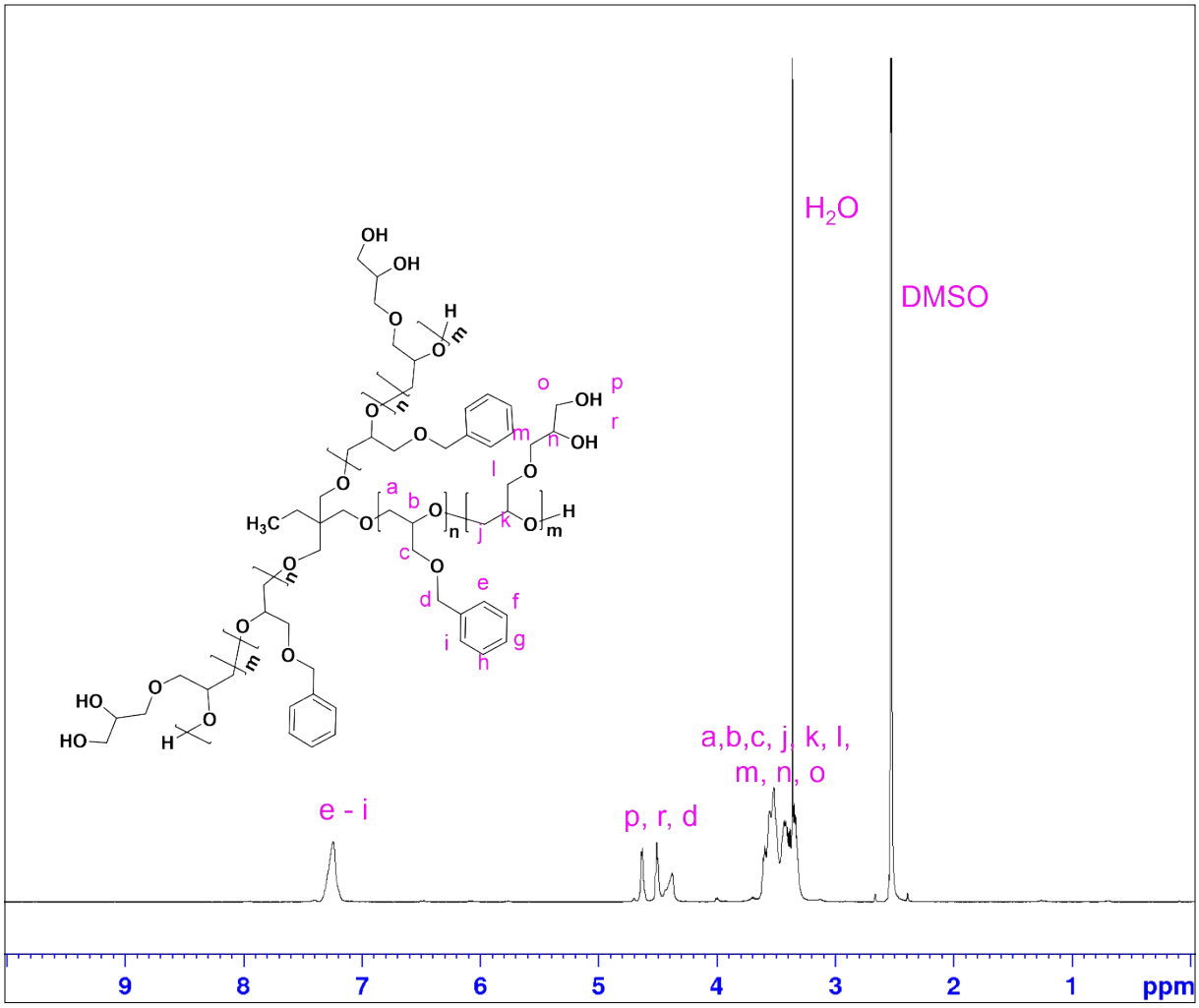

Figure S3. ^{1}H NMR spectrum of PBGE-PGGE_1 recorded in DMSO-d_6.

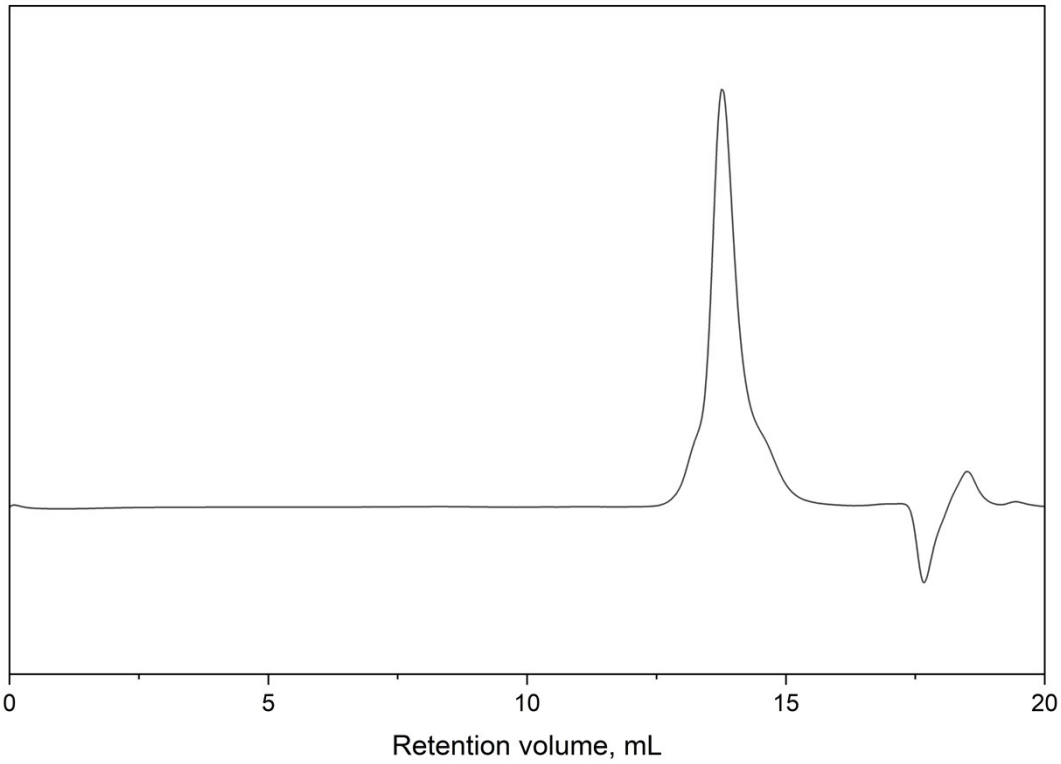

Figure S4. GPC chromatogram performed for PBGE-PGGE_1 copolyether. The analysis was performed using a chromatography system comprising components from Shimadzu/Wyatt, equipped with a RI Wyatt Optilab T-rEX (model: WTREX-04) and a set of columns (Agilent LC Columns, PLGel 5um Mixed-C 300x7.5mm) in a series configuration. Other components of the system included: a SHIMADZU LC-20 pump (model: RESERVOIR TRAY), a SHIMADZU degasser (model: DGU-20A5A), a SHIMADZU column oven (model: CTO-10ACvp), and a SHIMADZU autosampler (model: SIL-20AHT). N,N- dimethylacetamide (DMAc) was used as the eluent at a flow rate of 0.8 mL/min. Measurements were performed under the following temperature conditions: detector temperature - 25°C, column oven temperature - 40°C.

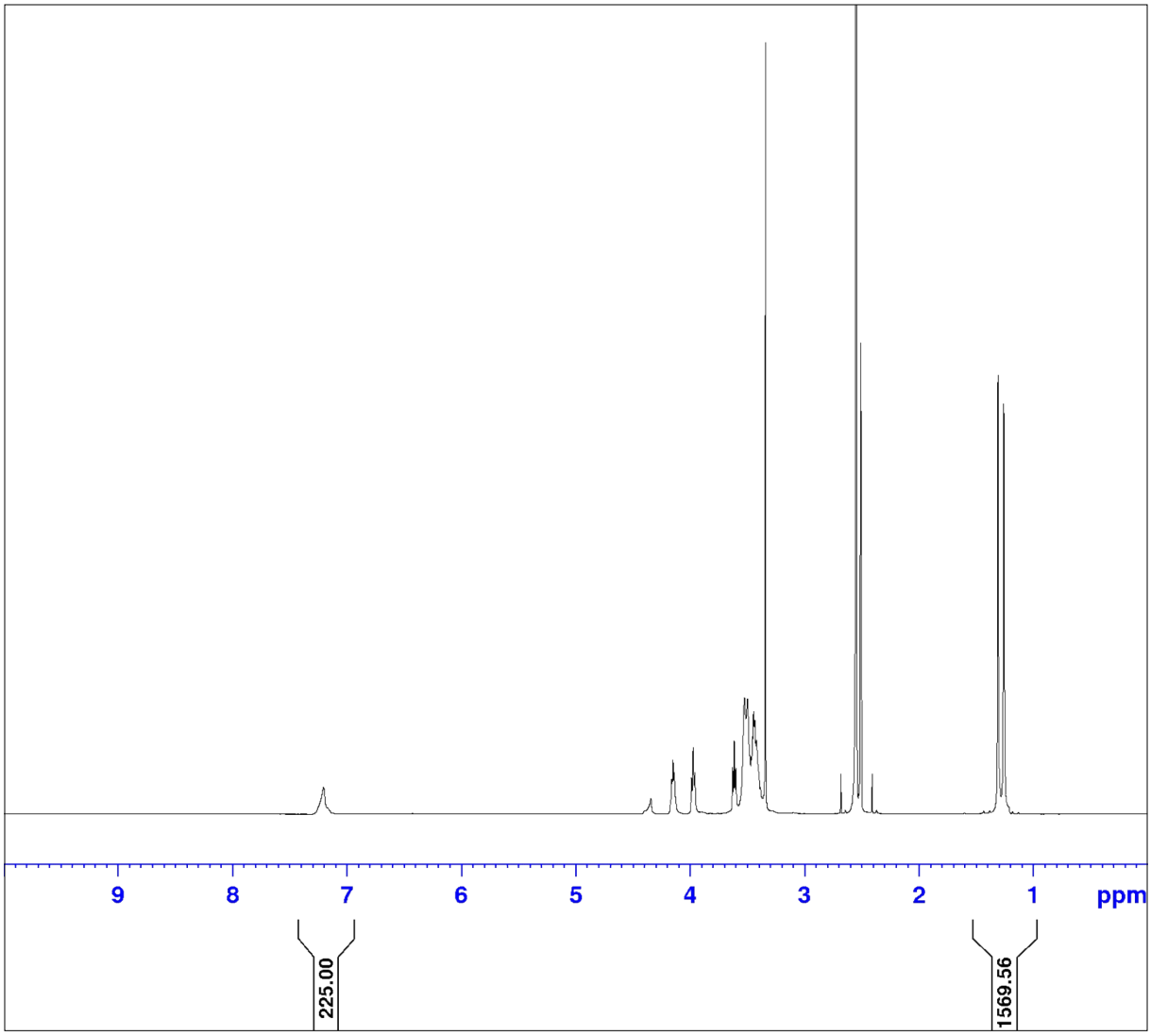

Figure S5. ^{1}H NMR spectrum of PBGE-PIGGE_2 recorded in DMSO-d_6.

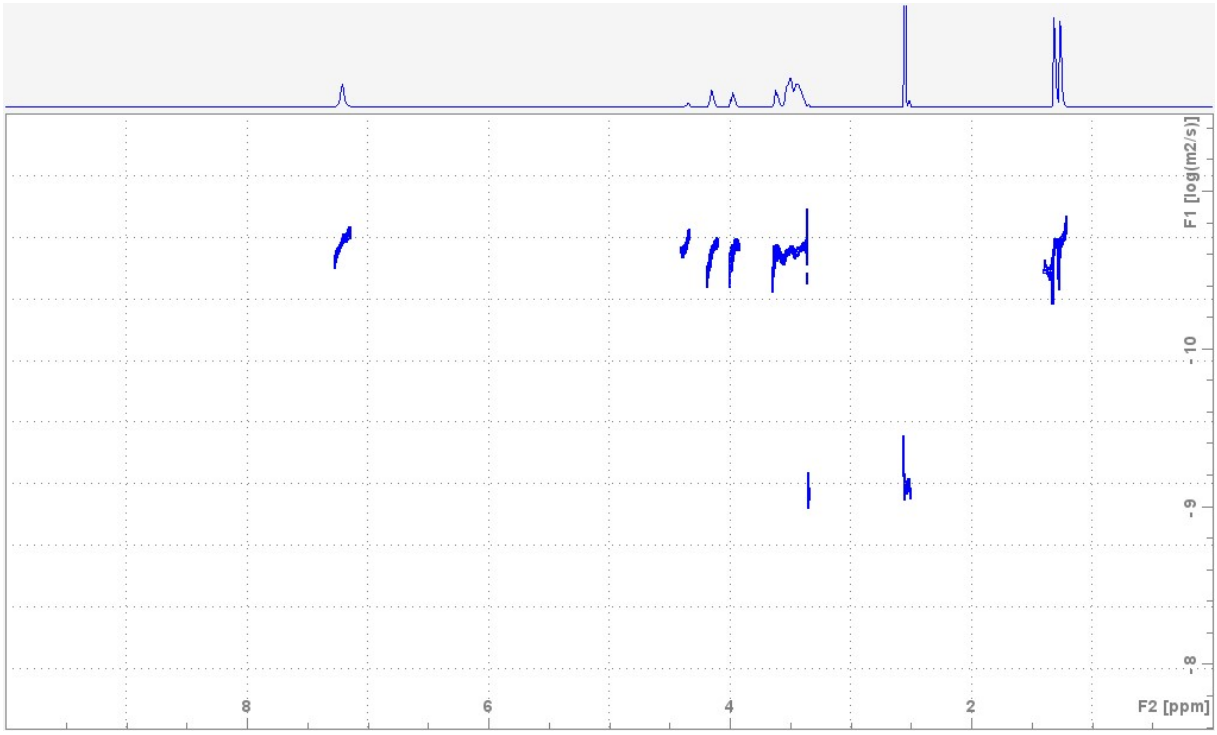

Figure S6. ^{1}H DOSY NMR spectrum of PBGE-PIGGE_2 recorded in DMSO-d_6.

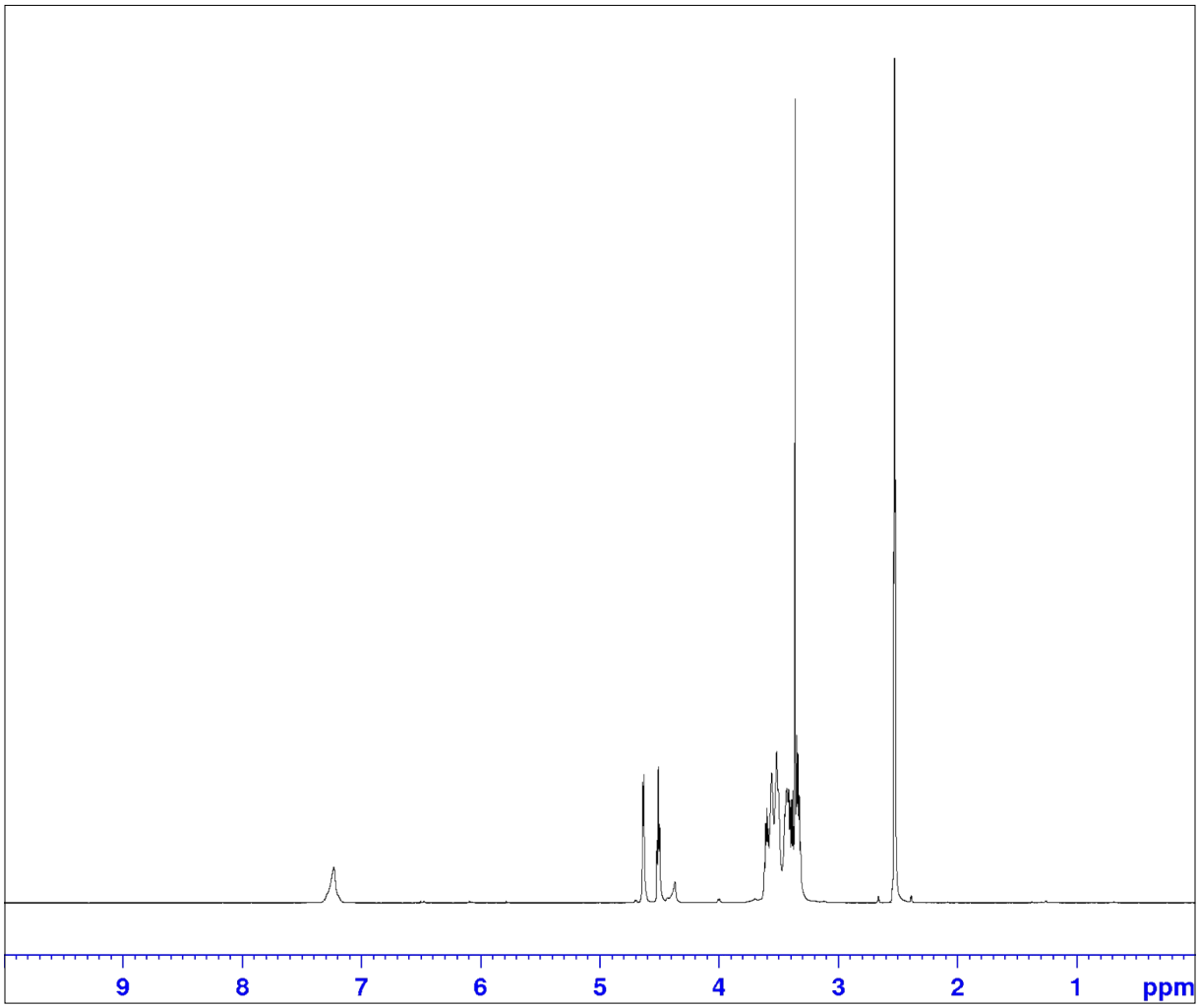

Figure S7. ^{1}H NMR spectrum of PBGE-PGGE_2 recorded in DMSO-d_6.

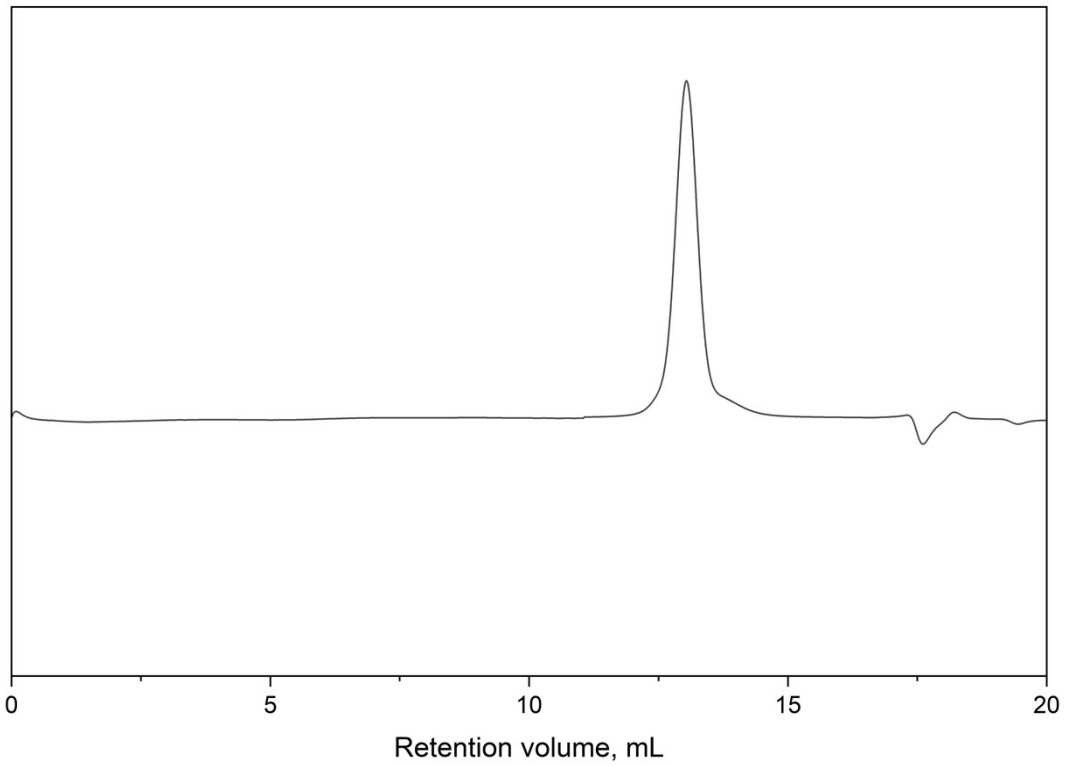

Figure S8. GPC chromatogram performed for PBGE-PGGE_2 copolyether. The analysis was performed using a chromatography system comprising components from Shimadzu/Wyatt, equipped with a RI Wyatt Optilab T-rEX (model: WTREX-04) and a set of columns (Agilent LC Columns, PLGel 5um Mixed-C 300x7.5mm) in a series configuration. Other components of the system included: a SHIMADZU LC-20 pump (model: RESERVOIR TRAY), a SHIMADZU degasser (model: DGU-20A5A), a SHIMADZU column oven (model: CTO-10ACvp), and a SHIMADZU autosampler (model: SIL-20AHT). N,N- dimethylacetamide (DMAc) was used as the eluent at a flow rate of 0.8 mL/min. Measurements were performed under the following temperature conditions: detector temperature - 25°C, column oven temperature - 40°C.

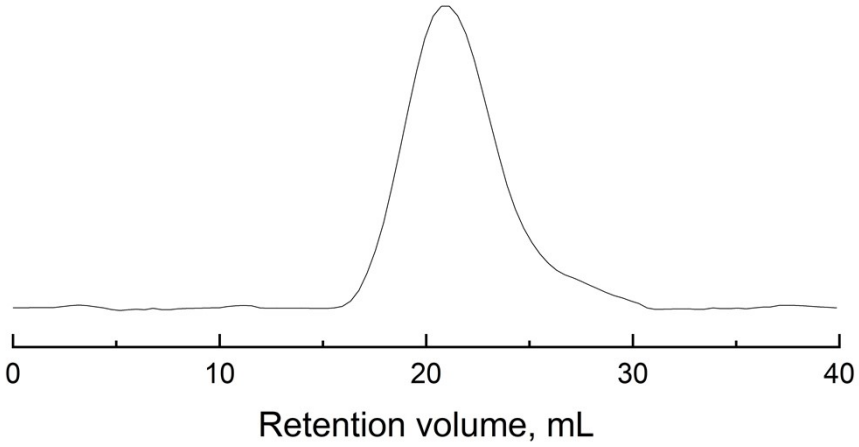

Figure S9. GPC chromatogram of poly(AM-*ran*-2-AAPBA)_1 performed in an aqueous solution at a flow rate of 1.0 mL min using a chromatograph (Knauer K-501 HPLC pump) equipped with a degasser (4-Channel Degasser; K-5004, Knauer), three TSK-GEL columns: G5000 PW XL 1 3000 PW XL 1 2500 PW XL (7.8 3 300 mm; Tosho; 26 8C), an LDC RI detector. Poly(ethylene oxide) was used as a standard.

Biological Investigations

Complete statistical data, including median distribution graphs of body weight and tumor volume measurement results for all groups participating in the experiment:

Table S1. *P*-values from statistical comparisons of body weight between the analyzed groups are presented. Values meeting the significance criterion ($p < 0.01$ to avoid false positive results) are highlighted in red.

Body weight [g]	PBGE-PGGE_1_NIF	PBGE-PGGE_2_NIF	PBGE-PGGE_1_NIF_gel	PBGE-PGGE_2_NIF_gel	Nifuratel	Placebo
PBGE-PGGE_1_NIF		0.277	1.000	<0.001	1.000	1.000
PBGE-PGGE_2_NIF	0.277		1.000	0.013	0.069	0.264
PBGE-PGGE_1_NIF_gel	1.000	1.000		0.001	0.726	1.000
PBGE-PGGE_2_NIF_gel	<0.001	0.013	0.001		<0.001	<0.001
Nifuratel	1.000	0.069	0.726	<0.001		1.000
Placebo	1.000	0.264	1.000	<0.001	1.000	

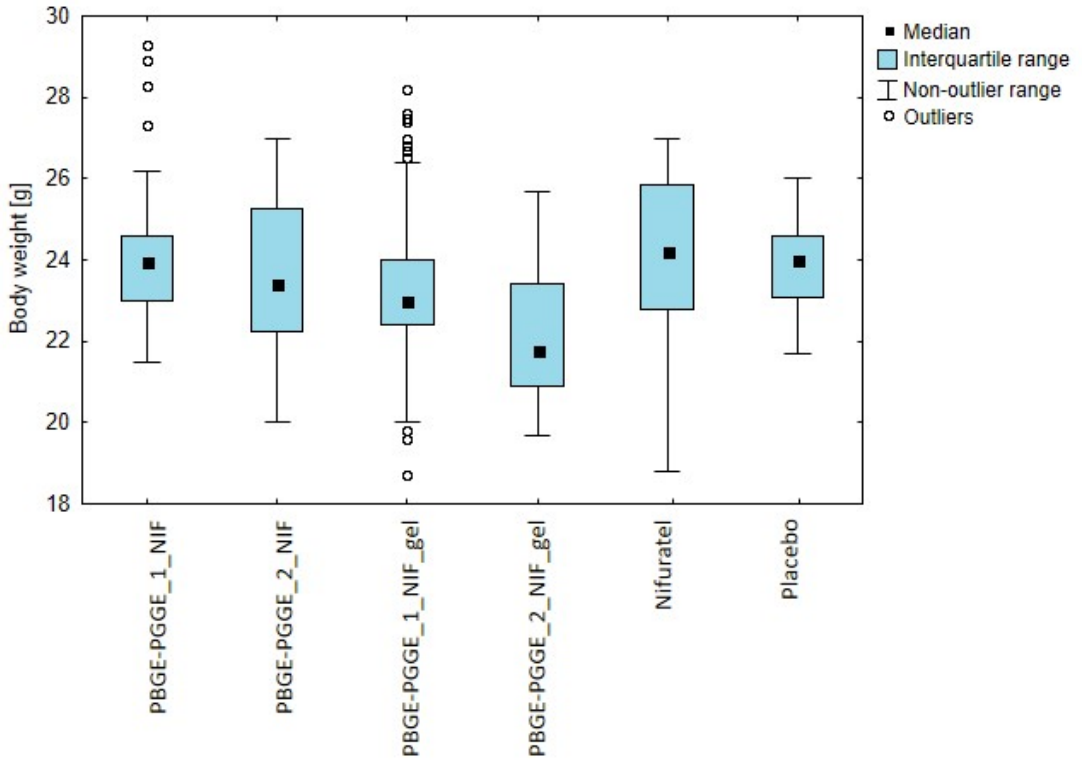

Figure S10. Boxplot show body weight [g] in each group. The square within each box represents the median value, while the box spans the interquartile range (25th–75th percentile). The whiskers extend to the most extreme data that are not classified as outliers (≤1.5 × IQR).

Table S2. *P*-values from statistical comparisons of tumor volume between the analyzed groups are presented. Values meeting the significance criterion ($p < 0.01$) are highlighted in red.

Tumor volume [mm³]	PBGE-PGGE_1_NIF	PBGE-PGGE_2_NIF	PBGE-PGGE_1_NIF_gel	PBGE-PGGE_2_NIF_gel	Nifuratel	Placebo
PBGE-PGGE_1_NIF		1.000	1.000	1.000	<0.001	<0.001
PBGE-PGGE_2_NIF	1.000		1.000	1.000	<0.001	<0.001
PBGE-PGGE_1_NIF_gel	1.000	1.000		1.000	0.002	<0.001
PBGE-PGGE_2_NIF_gel	1.000	1.000	1.000		<0.001	<0.001
Nifuratel	<0.001	<0.001	0.002	<0.001		0.717
Placebo	<0.001	<0.001	<0.001	<0.001	0.717	

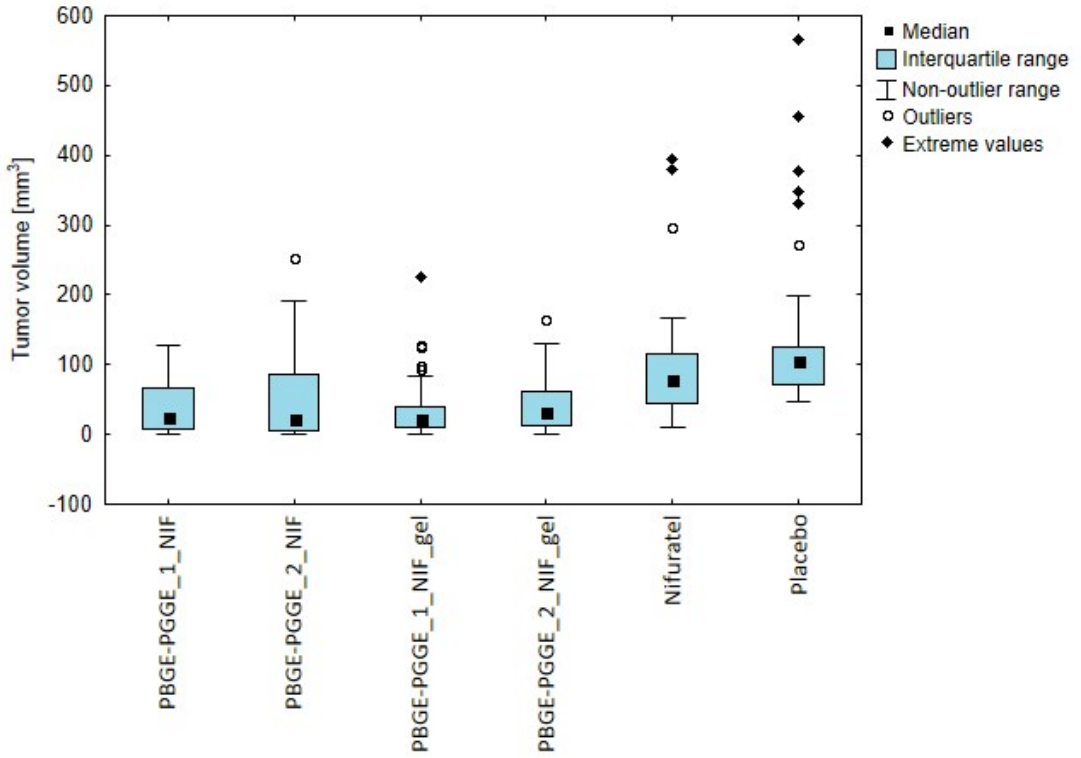

Figure S11. The box plot shows tumor volume [mm³] in each group. The square within each box represents the median value, while the box spans the interquartile range (25th–75th percentile). The whiskers extend to the most extreme data that are not classified as outliers (≤1.5 × IQR).

The following biochemical parameters were determined from the blood collected during the euthanasia of the mice: the level of lactate dehydrogenase (LDH), which indicates cell damage or death in the body,

the level of alanine aminotransferase (ALAT), which indicates liver condition, the level of aspartate aminotransferase (AST), which is crucial for metabolism and indicates liver, heart and skeletal muscle condition, the level of urea, which indicates kidney function (the ability to filter blood), as well as protein metabolism, body hydration and liver condition, the level of creatinine, which indicates kidney efficiency, the level of alkaline phosphatase (ALP), which indicates liver, bile duct and bone condition, the level of creatine kinase (CK), which indicates cellular tissue damage, the level of amylase, which indicates the condition of the pancreas and salivary glands, the level of CRP (C-reactive protein), which indicates the presence and severity of inflammation in the body, the level of albumin, which indicates liver health, kidney function, nutritional status and inflammation, the globulin level, which indicate inflammation, immunity, liver and kidney diseases and malnutrition, and total protein level, which indicate overall health, nutritional status and liver and kidney function.

Table S3. *P*-values from statistical comparisons of LDH between the analyzed groups are presented. Values meeting the significance criterion ($p < 0.01$) are highlighted in red.

LDH [U/l]	PBGE-PGGE_1_NIF	PBGE-PGGE_2_NIF	PBGE-PGGE_1_NIF_gel	PBGE-PGGE_2_NIF_gel	Nifuratel	Placebo
PBGE-PGGE_1_NIF		1.000	1.000	1.000	1.000	1.000
PBGE-PGGE_2_NIF	1.000		0.536	1.000	1.000	1.000
PBGE-PGGE_1_NIF_gel	1.000	0.536		1.000	1.000	1.000
PBGE-PGGE_2_NIF_gel	1.000	1.000	1.000		1.000	1.000
Nifuratel	1.000	1.000	1.000	1.000		1.000
Placebo	1.000	1.000	1.000	1.000	1.000	

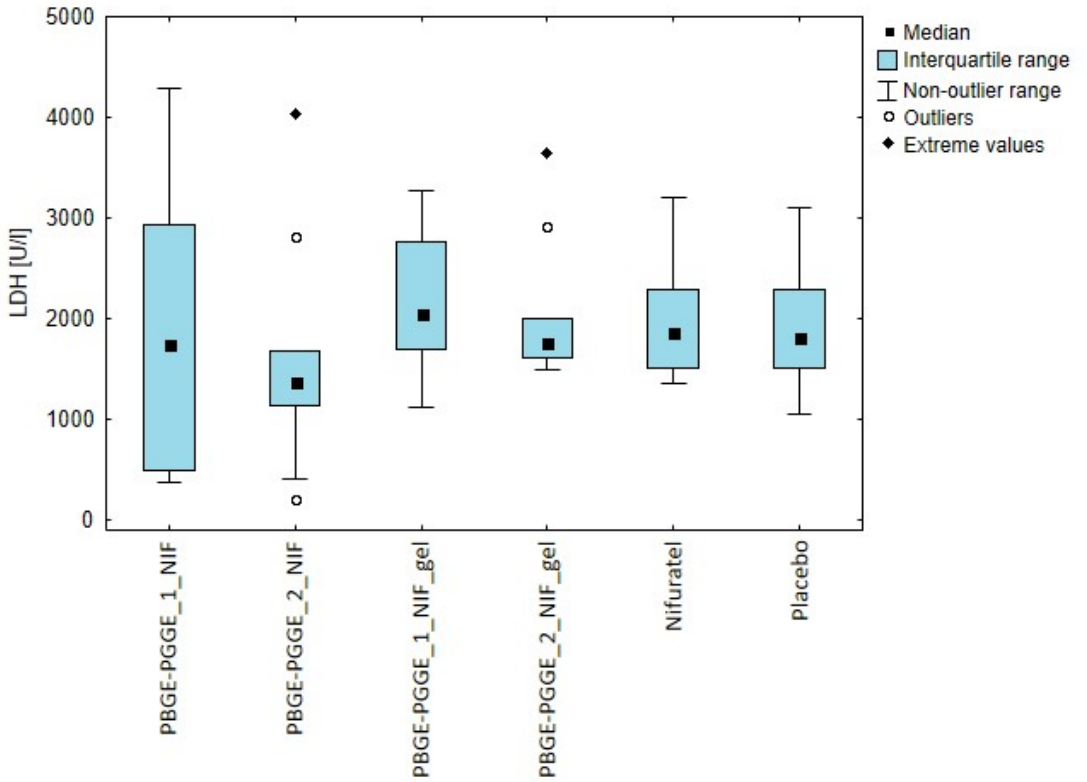

Figure S12. Boxplot show LDH levels [U/l] in each group. The square within each box represents the median value, while the box spans the interquartile range (25th–75th percentile). The whiskers extend to the most extreme data that are not classified as outliers (≤1.5 × IQR).

Table S4. *P*-values from statistical comparisons of ALAT between the analyzed groups are presented. Values meeting the significance criterion ($p < 0.01$) are highlighted in red.

ALAT [U/l]	PBGE-PGGE_1_NIF	PBGE-PGGE_2_NIF	PBGE-PGGE_1_NIF_gel	PBGE-PGGE_2_NIF_gel	Nifuratel	Placebo
PBGE-PGGE_1_NIF		1.000	0.035	0.617	0.846	0.030
PBGE-PGGE_2_NIF	1.000		0.047	0.775	1.000	0.042
PBGE-PGGE_1_NIF_gel	0.035	0.047		1.000	1.000	1.000
PBGE-PGGE_2_NIF_gel	0.617	0.775	1.000		1.000	1.000
Nifuratel	0.846	1.000	1.000	1.000		1.000
Placebo	0.030	0.042	1.000	1.000	1.000	

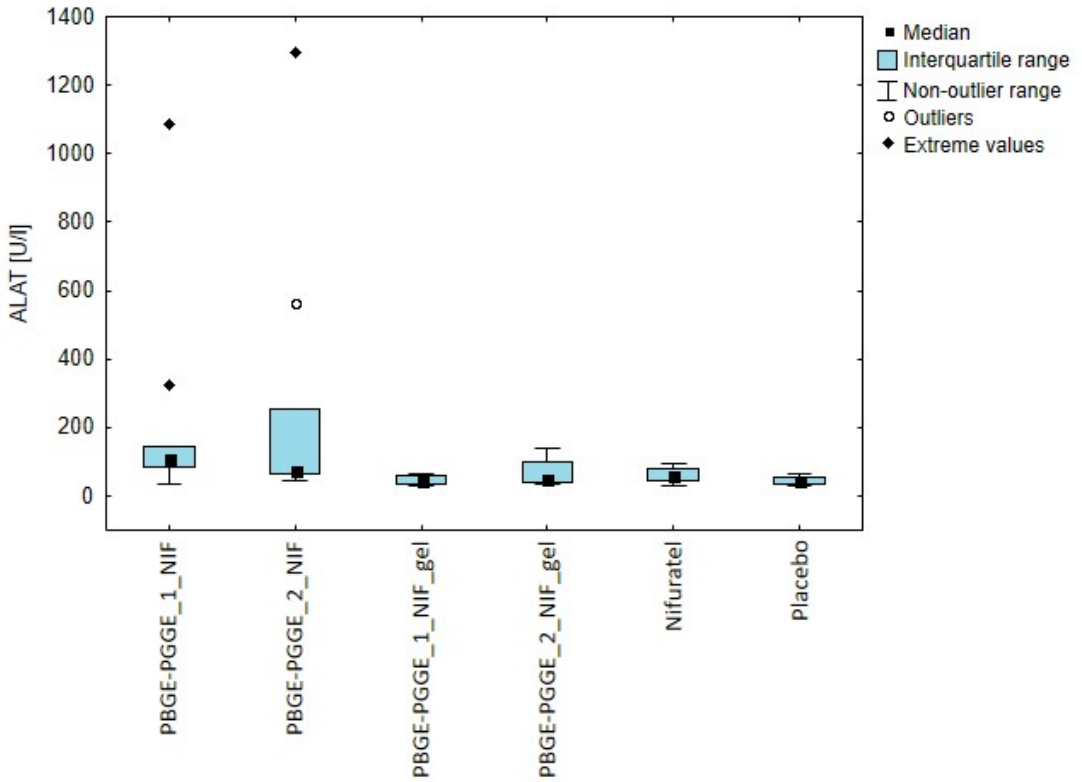

Figure S13. Boxplot show ALAT levels [U/l] in each group. The square within each box represents the median value, while the box spans the interquartile range (25th–75th percentile). The whiskers extend to the most extreme data that are not classified as outliers (≤1.5 × IQR).

Table S5. *P*-values from statistical comparisons of ASPAT between the analyzed groups are presented. Values meeting the significance criterion ($p < 0.01$) are highlighted in red.

ASPAT [U/l]	PBGE-PGGE_1_NIF	PBGE-PGGE_2_NIF	PBGE-PGGE_1_NIF_gel	PBGE-PGGE_2_NIF_gel	Nifuratel	Placebo
PBGE-PGGE_1_NIF		1.000	0.135	1.000	0.503	0.646
PBGE-PGGE_2_NIF	1.000		0.307	1.000	1.000	1.000
PBGE-PGGE_1_NIF_gel	0.135	0.307		0.217	1.000	1.000
PBGE-PGGE_2_NIF_gel	1.000	1.000	0.217		0.752	0.950
Nifuratel	0.503	1.000	1.000	0.752		1.000

Placebo	0.646	1.000	1.000	0.950	1.000	

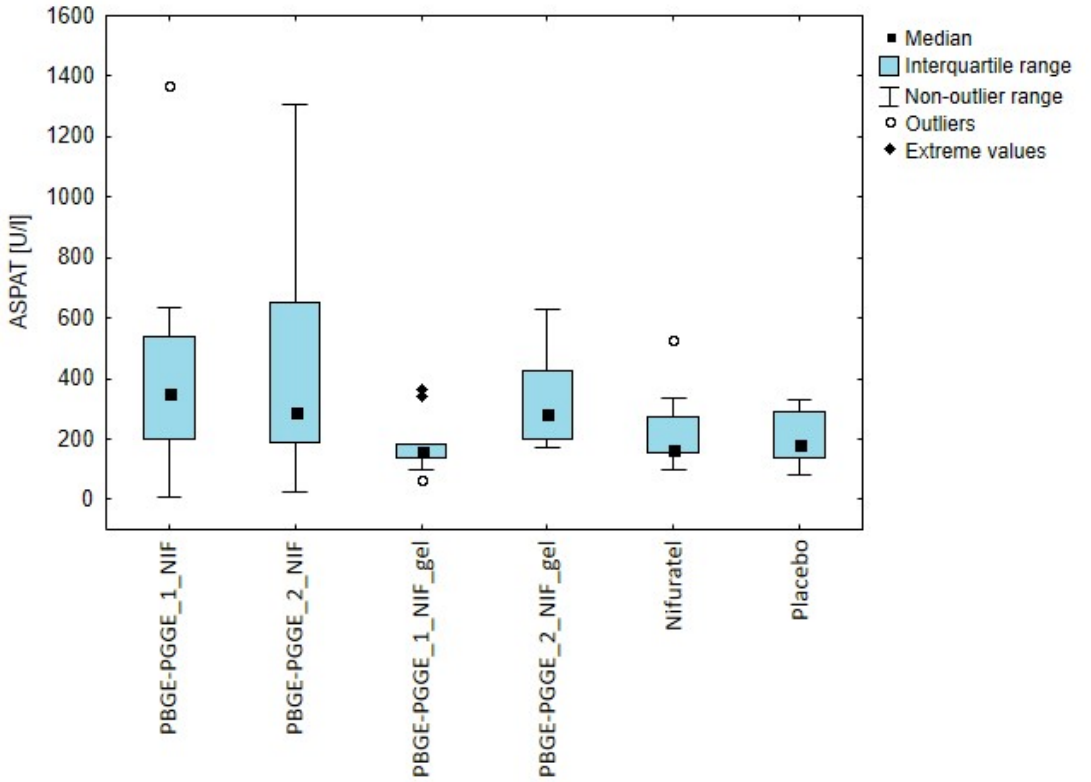

Figure S14. Boxplot show ASPAT levels [U/l] in each group. The square within each box represents the median value, while the box spans the interquartile range (25th–75th percentile). The whiskers extend to the most extreme data that are not classified as outliers (≤1.5 × IQR).

Table S6. *P*-values from statistical comparisons of urea between the analyzed groups are presented. Values meeting the significance criterion ($p < 0.01$) are highlighted in red.

Urea [mg/dl]	PBGE-PGGE_1_NIF	PBGE-PGGE_2_NIF	PBGE-PGGE_1_NIF_gel	PBGE-PGGE_2_NIF_gel	Nifuratel	Placebo
PBGE-PGGE_1_NIF		1.000	1.000	1.000	1.000	1.000
PBGE-PGGE_2_NIF	1.000		1.000	1.000	1.000	1.000

PBGE-PGGE_1_NIF_gel	1.000	1.000		1.000	1.000	1.000
PBGE-PGGE_2_NIF_gel	1.000	1.000	1.000		1.000	1.000
Nifuratel	1.000	1.000	1.000	1.000		0.401
Placebo	1.000	1.000	1.000	1.000	0,401	

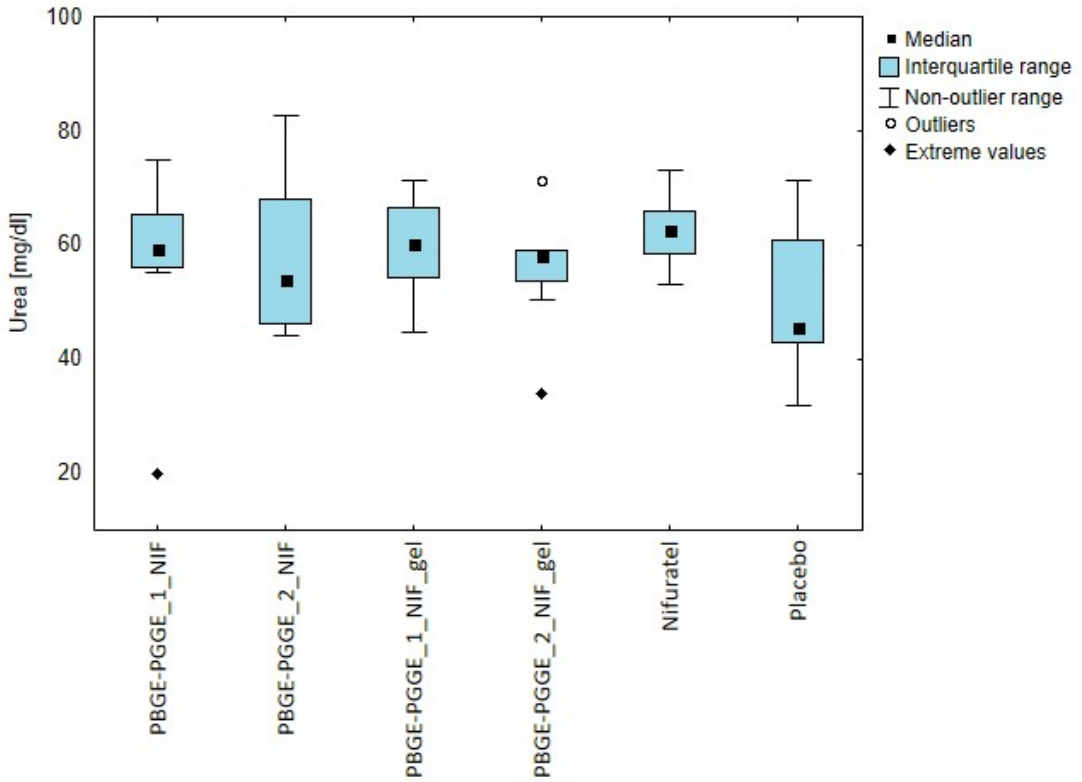

Figure S15. Boxplot show urea levels [mg/dl] in each group. The square within each box represents the median value, while the box spans the interquartile range (25th–75th percentile). The whiskers extend to the most extreme data that are not classified as outliers (≤1.5 × IQR).

Table S7. *P*-values from statistical comparisons of creatinine between the analyzed groups are presented. Values meeting the significance criterion ($p < 0.01$) are highlighted in red.

Creatinine [mg/dl]	PBGE-PGGE_1_NIF	PBGE-PGGE_2_NIF	PBGE-PGGE_1_NIF_gel	PBGE-PGGE_2_NIF_gel	Nifuratel	Placebo
PBGE-PGGE_1_NIF		1.000	0.553	0.110	1.000	1.000
PBGE-PGGE_2_NIF	1.000		0.024	1.000	0.073	0.195
PBGE-PGGE_1_NIF_gel	0.553	0.024		<0.001	1.000	1.000
PBGE-PGGE_2_NIF_gel	0.110	1.000	<0.001		<0.001	<0.001
Nifuratel	1.000	0.073	1.000	<0.001		1.000
Placebo	1.000	0.195	1.000	<0.001	1.000	

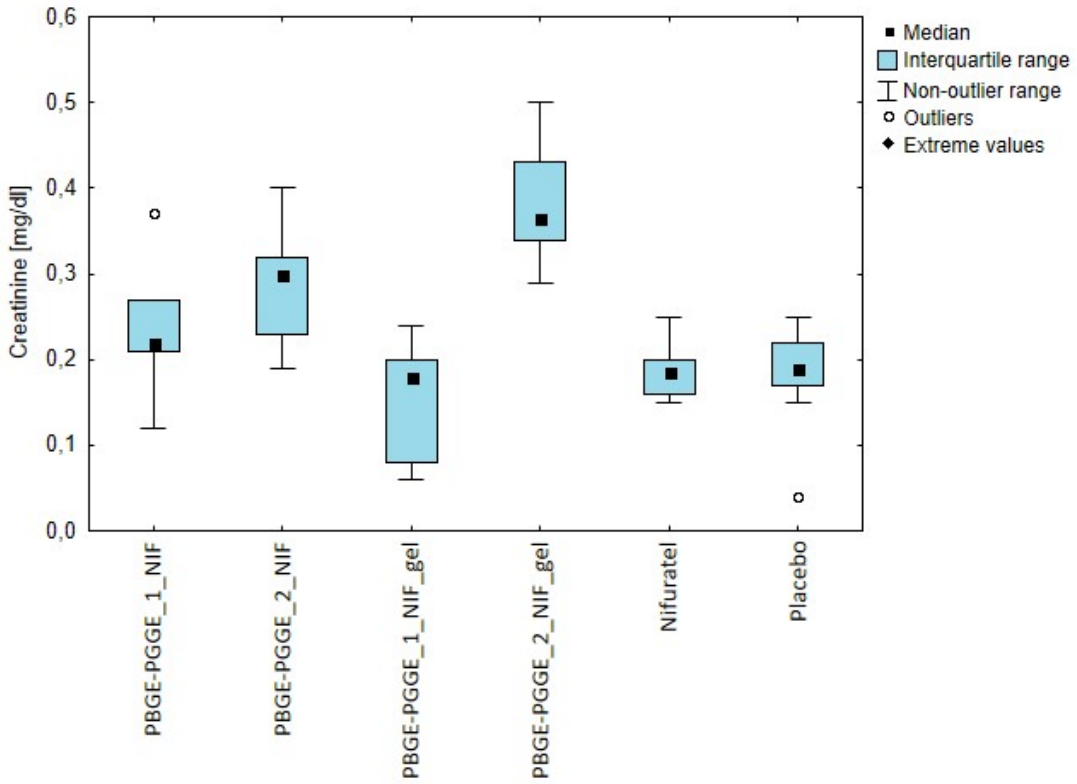

Figure S16. Boxplot show creatinine levels [mg/dl] in each group. The square within each box represents the median value, while the box spans the interquartile range (25th–75th percentile). The whiskers extend to the most extreme data that are not classified as outliers (≤1.5 × IQR).

Table S8. *P*-values from statistical comparisons of alkaline phosphatase between the analyzed groups are presented. Values meeting the significance criterion ($p < 0.01$) are highlighted in red.

Alkaline phosphatase [U/l]	PBGE-PGGE_1_NIF	PBGE-PGGE_2_NIF	PBGE-PGGE_1_NIF_gel	PBGE-PGGE_2_NIF_gel	Nifuratel	Placebo
PBGE-PGGE_1_NIF		1.000	0.229	1.000	1.000	0.006
PBGE-PGGE_2_NIF	1.000		1.000	1.000	1.000	0.063
PBGE-PGGE_1_NIF_gel	0.229	1.000		1.000	1.000	1.000
PBGE-PGGE_2_NIF_gel	1.000	1.000	1.000		1.000	0.202
Nifuratel	1.000	1.000	1.000	1.000		0.146
Placebo	0.006	0.063	1.000	0.202	0.146	

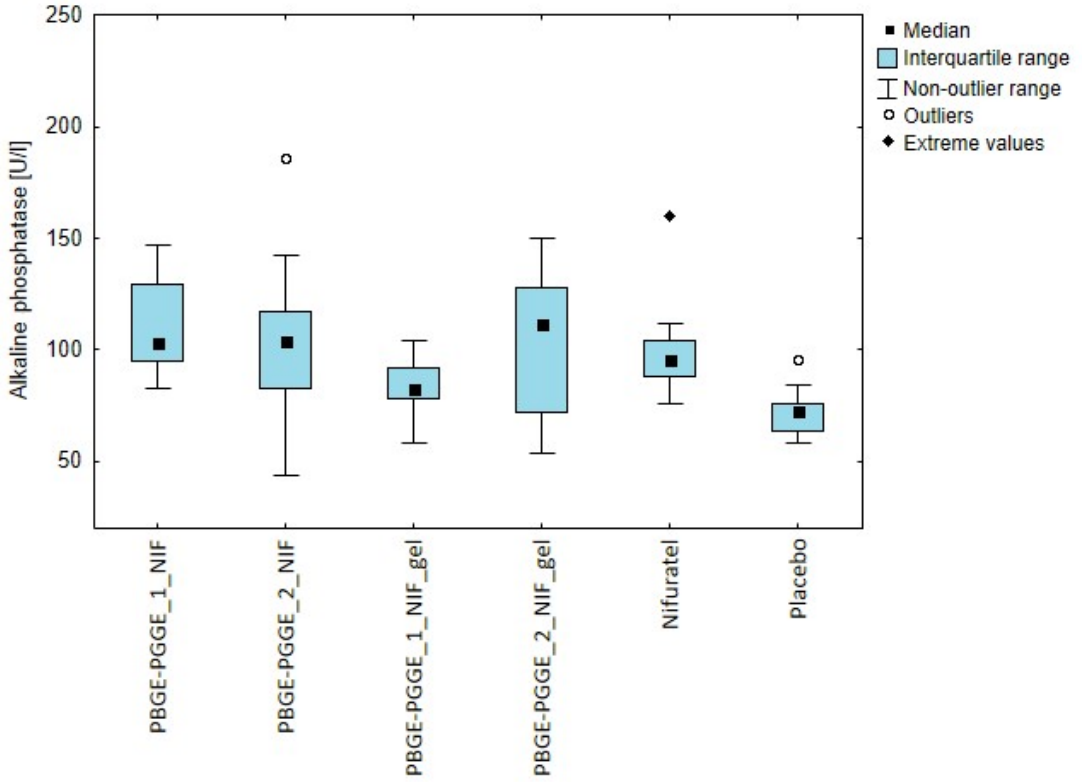

Figure S17. Boxplot show alkaline phosphatase levels [U/l] in each group. The square within each box represents the median value, while the box spans the interquartile range (25th–75th percentile). The whiskers extend to the most extreme data that are not classified as outliers (≤1.5 × IQR).

Table S9. *P*-values from statistical comparisons of creatine kinase between the analyzed groups are presented. Values meeting the significance criterion ($p < 0.01$) are highlighted in red.

Creatine kinase [U/l]	PBGE-PGGE_1_NIF	PBGE-PGGE_2_NIF	PBGE-PGGE_1_NIF_gel	PBGE-PGGE_2_NIF_gel	Nifuratel	Placebo
PBGE-PGGE_1_NIF		1.000	0.217	1.000	1.000	0.608
PBGE-PGGE_2_NIF	1.000		0.073	1.000	0.428	0.233
PBGE-PGGE_1_NIF_gel	0.217	0.073		0.163	1.000	1.000
PBGE-PGGE_2_NIF_gel	1.000	1.000	0.163		0.822	0.472
Nifuratel	1.000	0.428	1.000	0.822		1.000
Placebo	0.608	0.233	1.000	0.472	1.000	

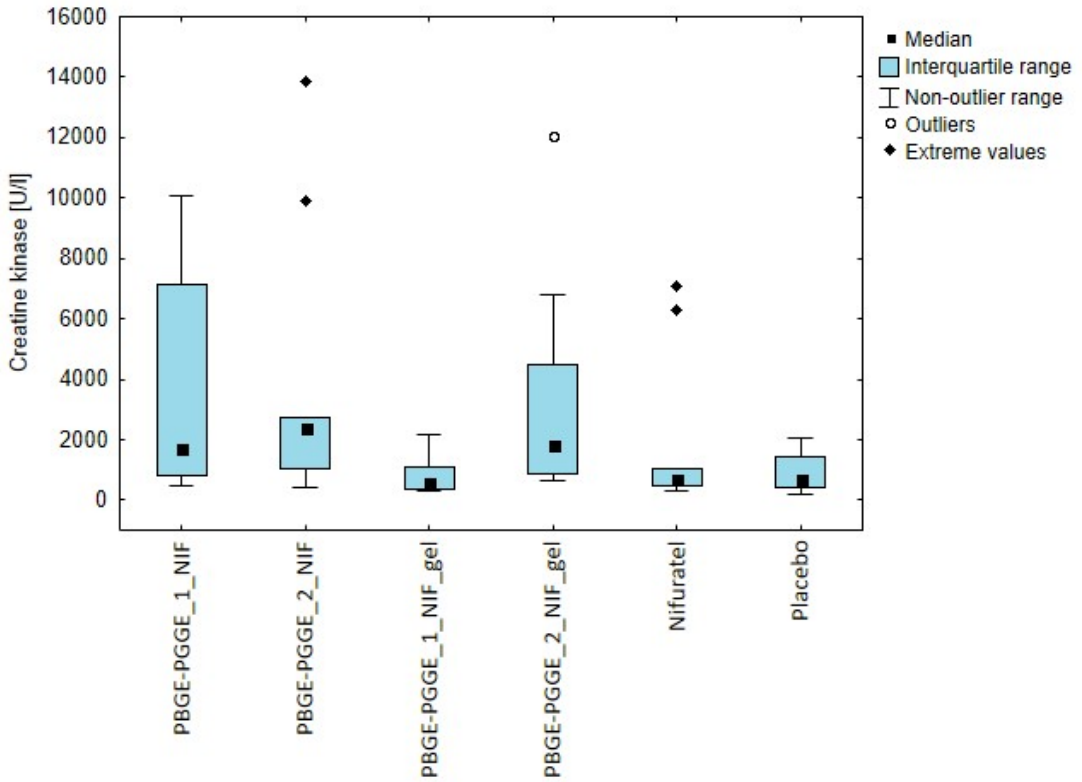

Figure S18. Boxplot show creatinine kinase levels [U/l] in each group. The square within each box represents the median value, while the box spans the interquartile range (25th–75th percentile). The whiskers extend to the most extreme data that are not classified as outliers (≤1.5 × IQR).

Table S10. *P*-values from statistical comparisons of amylase between the analyzed groups are presented. Values meeting the significance criterion ($p < 0.01$) are highlighted in red.

Amylase [U/l]	PBGE-PGGE_1_NIF	PBGE-PGGE_2_NIF	PBGE-PGGE_1_NIF_gel	PBGE-PGGE_2_NIF_gel	Nifuratel	Placebo
PBGE-PGGE_1_NIF		1.000	1.000	1.000	1.000	1.000
PBGE-PGGE_2_NIF	1.000		1.000	1.000	1.000	1.000
PBGE-PGGE_1_NIF_gel	1.000	1.000		1.000	1.000	1.000
PBGE-PGGE_2_NIF_gel	1.000	1.000	1.000		1.000	0.687
Nifuratel	1.000	1.000	1.000	1.000		1.000

Placebo	1.000	1.000	1.000	0.667	1.000	

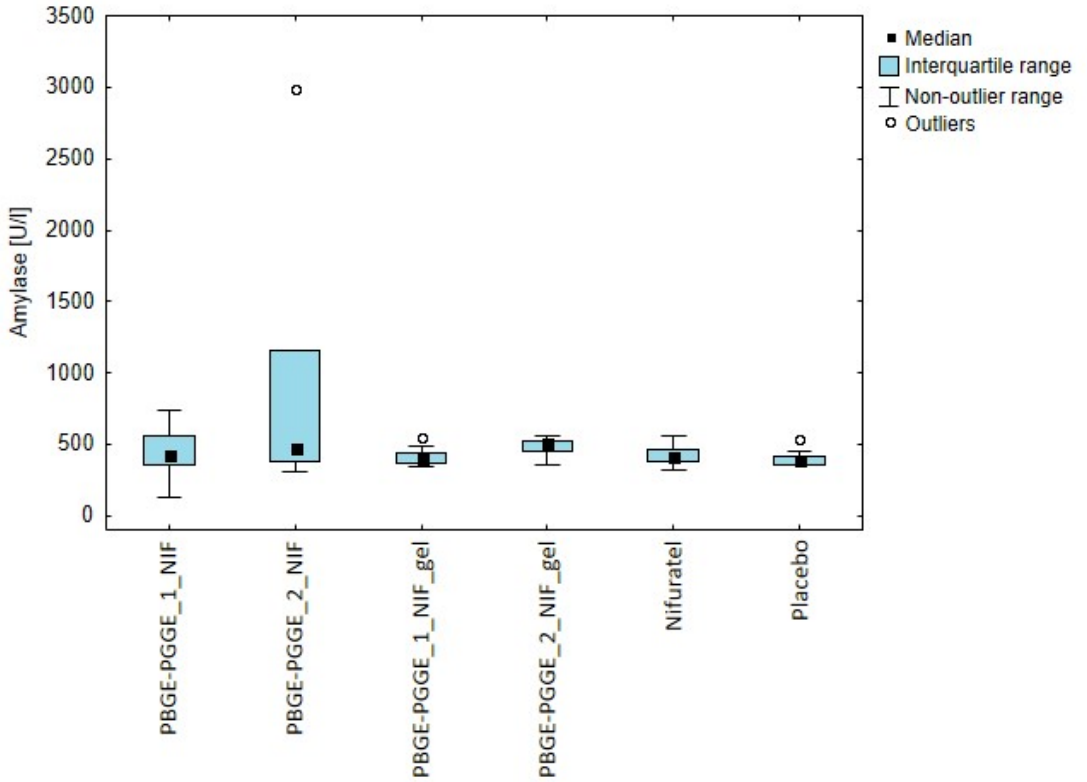

Figure S19. Boxplot show amylase levels [U/l] in each group. The square within each box represents the median value, while the box spans the interquartile range (25th–75th percentile). The whiskers extend to the most extreme data that are not classified as outliers (≤1.5 × IQR).

Table S11. *P*-values from statistical comparisons of CRP between the analyzed groups are presented. Values meeting the significance criterion ($p < 0.01$) are highlighted in red.

CRP [mg/l]	PBGE-PGGE_1_NIF	PBGE-PGGE_2_NIF	PBGE-PGGE_1_NIF_gel	PBGE-PGGE_2_NIF_gel	Nifuratel	Placebo
PBGE-PGGE_1_NIF		0.121	1.000	0.479	1.000	1.000
PBGE-PGGE_2_NIF	0.121		0.048	1.000	0.100	0.090

PBGE-PGGE_1_NIF_gel	1.000	0.048		0.221	1.000	1.000
PBGE-PGGE_2_NIF_gel	0.479	1.000	0.221		0.408	0.376
Nifuratel	1.000	0.100	1.000	0.408		1.000
Placebo	1.000	0.090	1.000	0.376	1.000	

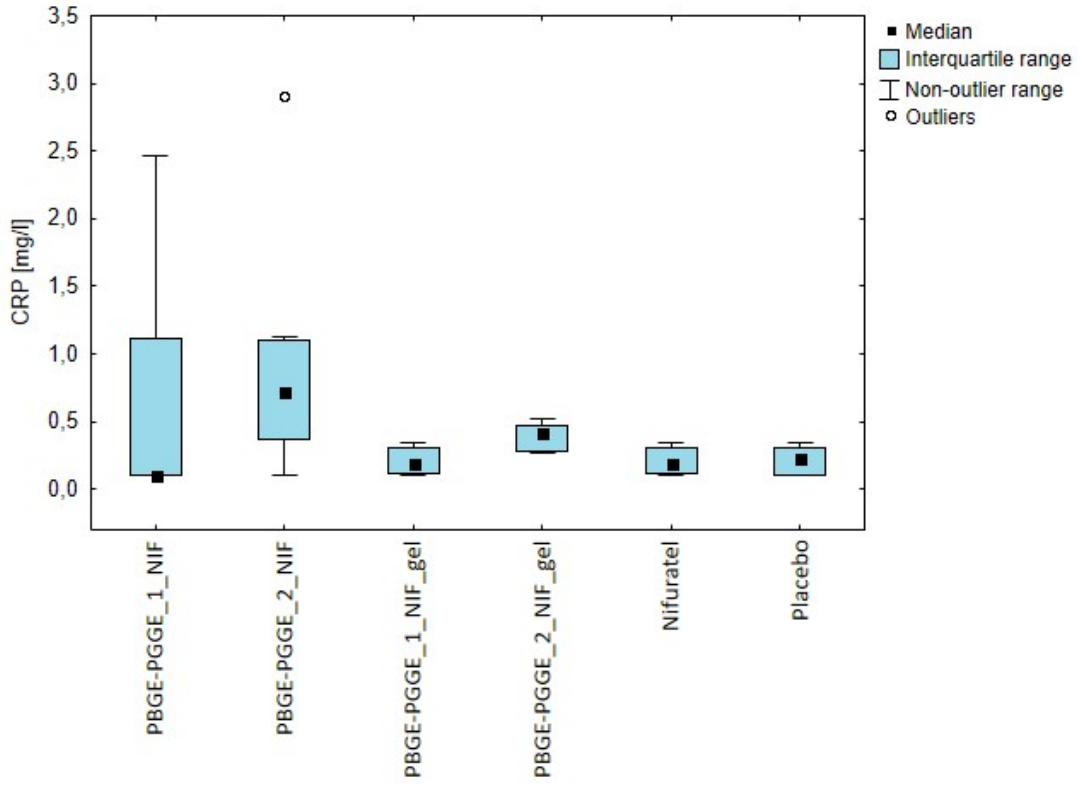

Figure S20. Boxplot show CRP levels [mg/l] in each group. The square within each box represents the median value, while the box spans the interquartile range (25th–75th percentile). The whiskers extend to the most extreme data that are not classified as outliers (≤1.5 × IQR).

Table S12. *P*-values from statistical comparisons of albumine between the analyzed groups are presented. Values meeting the significance criterion ($p < 0.01$) are highlighted in red.

Albumin [g/l]	PBGE-PGGE_1_NIF	PBGE-PGGE_2_NIF	PBGE-PGGE_1_NIF_gel	PBGE-PGGE_2_NIF_gel	Nifuratel	Placebo
PBGE-PGGE_1_NIF		1.000	0.859	0.011	0.395	<0.001
PBGE-PGGE_2_NIF	1.000		1.000	0.281	1.000	0.003
PBGE-PGGE_1_NIF_gel	0.859	1.000		1.000	1.000	0.070
PBGE-PGGE_2_NIF_gel	0.011	0.282	1.000		1.000	1.000
Nifuratel	0.395	1.000	1.000	1.000		0.181
Placebo	<0.001	0.003	0.070	1.000	0.181	

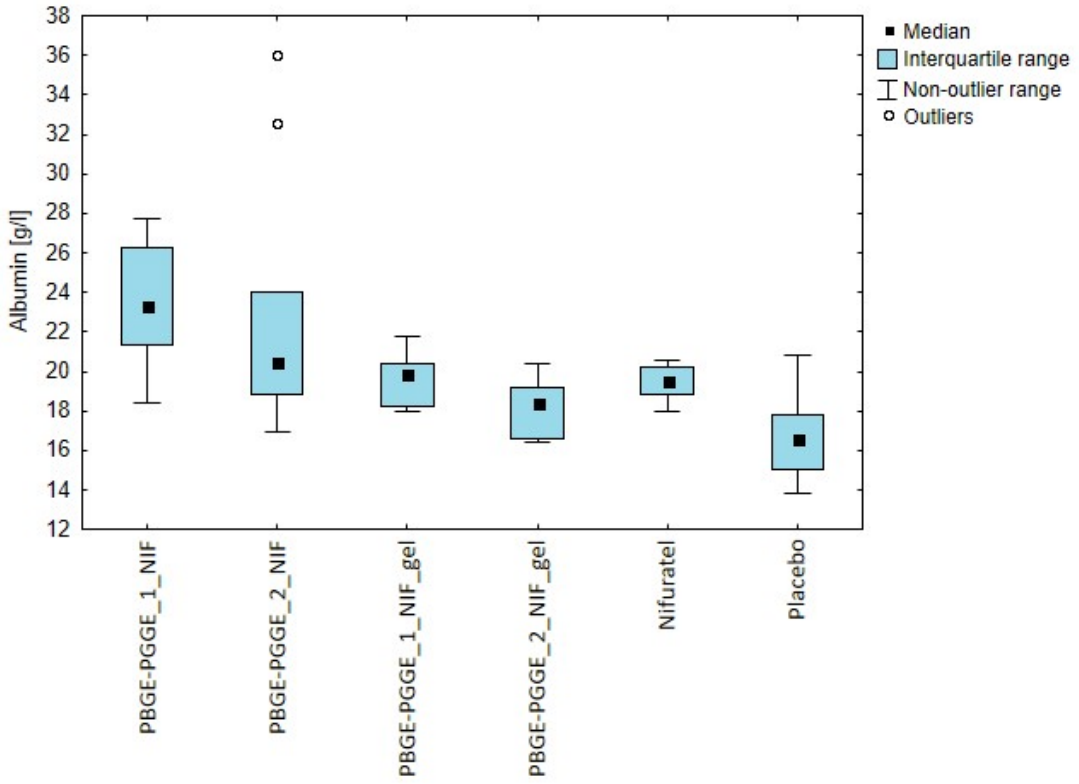

Figure S21. Boxplot show albumin levels [g/l] in each group. The square within each box represents the median value, while the box spans the interquartile range (25th–75th percentile). The whiskers extend to the most extreme data that are not classified as outliers (≤1.5 × IQR).

Table S13. *P*-values from statistical comparisons of globulins between the analyzed groups are presented. Values meeting the significance criterion ($p < 0.01$) are highlighted in red.

Globulins [g/l]	PBGE-PGGE_1_NIF	PBGE-PGGE_2_NIF	PBGE-PGGE_1_NIF_gel	PBGE-PGGE_2_NIF_gel	Nifuratel	Placebo
PBGE-PGGE_1_NIF		1.000	0.172	1.000	1.000	0.002
PBGE-PGGE_2_NIF	1.000		0.014	1.000	1.000	<0,001
PBGE-PGGE_1_NIF_gel	0.172	0.014		1.000	0.730	1.000
PBGE-PGGE_2_NIF_gel	1.000	1.000	1.000		1.000	0,054
Nifuratel	1.000	1.000	0.730	1.000		0.016
Placebo	0.002	<0.001	1.000	0.054	0.016	

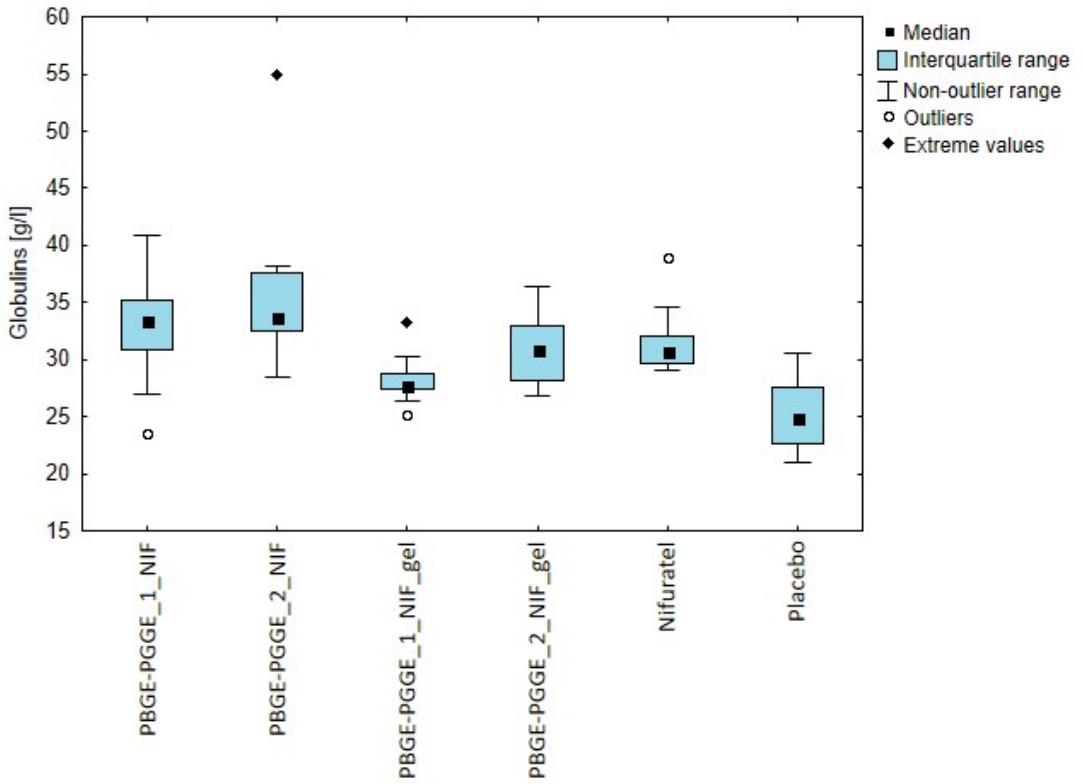

Figure S22. Boxplot show globulins levels [g/l] in each group. The square within each box represents the median value, while the box spans the interquartile range (25th–75th percentile). The whiskers extend to the most extreme data that are not classified as outliers (≤1.5 × IQR).

Table S14. *P*-values from statistical comparisons of total protein between the analyzed groups are presented. Values meeting the significance criterion ($p < 0.01$) are highlighted in red.

Total protein [g/dl]	PBGE-PGGE_1_NIF	PBGE-PGGE_2_NIF	PBGE-PGGE_1_NIF_gel	PBGE-PGGE_2_NIF_gel	Nifuratel	Placebo
PBGE-PGGE_1_NIF		1.000	0,687	1.000	1.000	0,004
PBGE-PGGE_2_NIF	1.000		0,042	0,598	1.000	<0.001
PBGE-PGGE_1_NIF_gel	0,687	0,042		1.000	1.000	1.000
PBGE-PGGE_2_NIF_gel	1.000	0,598	1.000		1.000	0,140
Nifuratel	1.000	1.000	1.000	1.000		0,014
Placebo	0,004	<0.001	1.000	0,140	0,014	

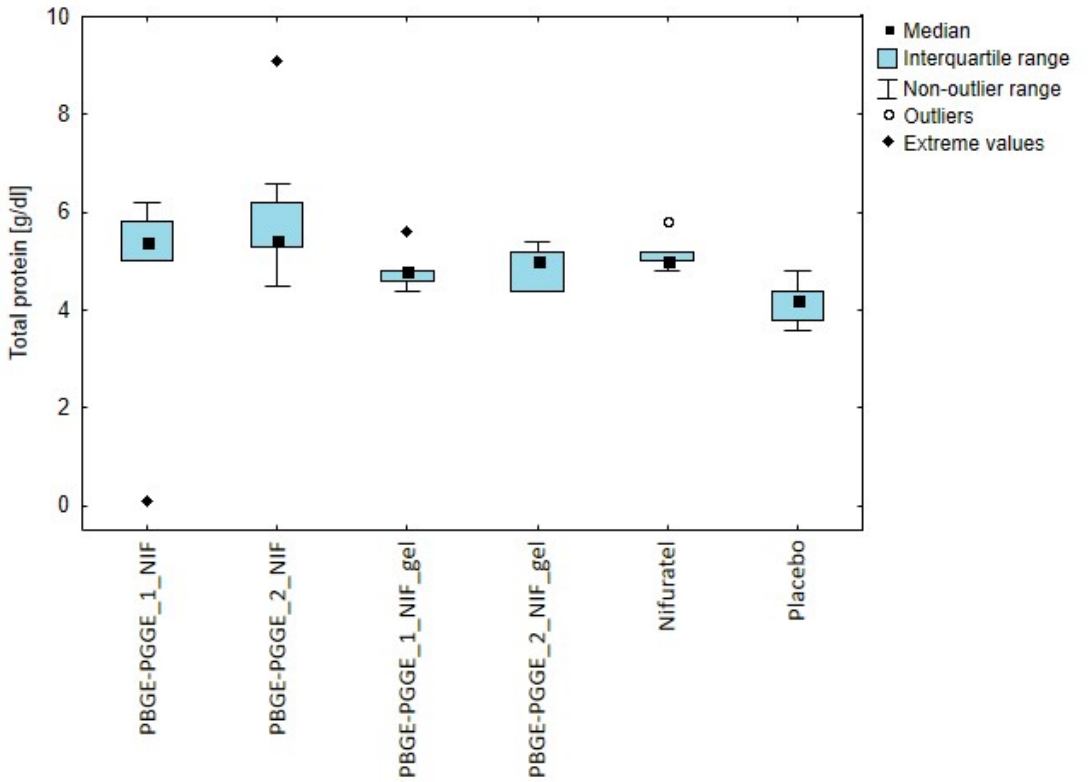

Figure S23. Boxplot show total protein levels [g/l] in each group. The square within each box represents the median value, while the box spans the interquartile range (25th–75th percentile). The whiskers extend to the most extreme data that are not classified as outliers (≤1.5 × IQR).

During euthanasia, the livers and tumors of the animals were collected for further analysis. The largest and smallest tumors from each study group, along with the liver, were selected for histopathological evaluation. In groups with comparable tumor sizes, one tumor was randomly selected for histopathological evaluation. Below, we present a compilation of photographs of tissue slides fixed in formalin, embedded in paraffin, sectioned, and stained with hematoxylin and eosin. To facilitate comparison of the results, a thumbnail image of each slide showing the tumor before fixation and the animal's number in the study group has been included.

PBGE-PGGE_1_NIF

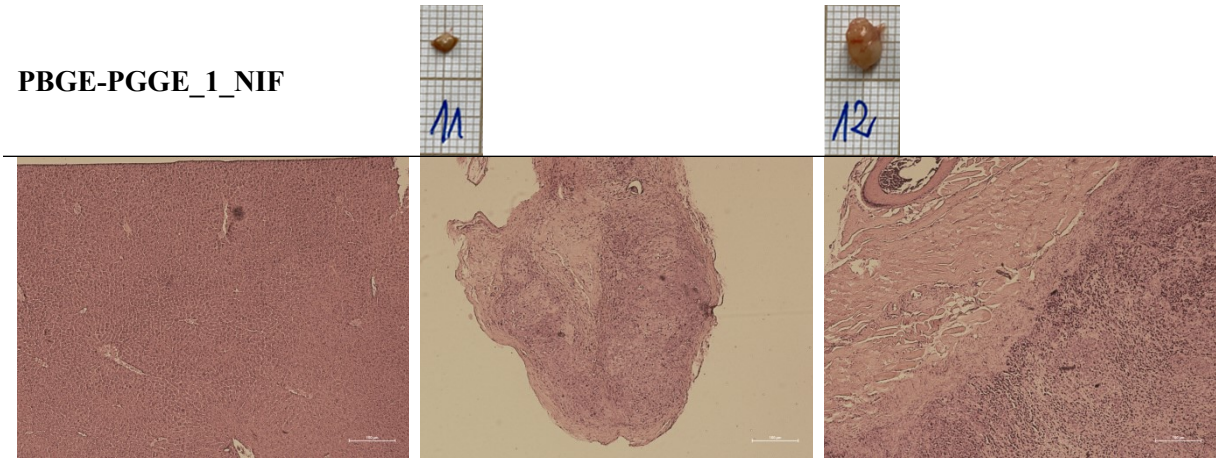

liver (12) tumor (11) tumor (12)

Liver (12): The lobular architecture is distorted due to vascular changes. However, the absence of bridging fibrosis or cirrhotic remodeling suggests that the organ may have been damaged during euthanasia/harvest.
Tumor (11): Malignant solid tumor composed of large anaplastic cells with abundant cytoplasm and large nuclei with prominent eosinophilic nucleoli.
Tumor (12): Malignant solid tumor composed of small cells with scant cytoplasm and hyperchromatic nuclei with 'pepper and salt' chromatin.

PBGE-PGGE_2_NIF

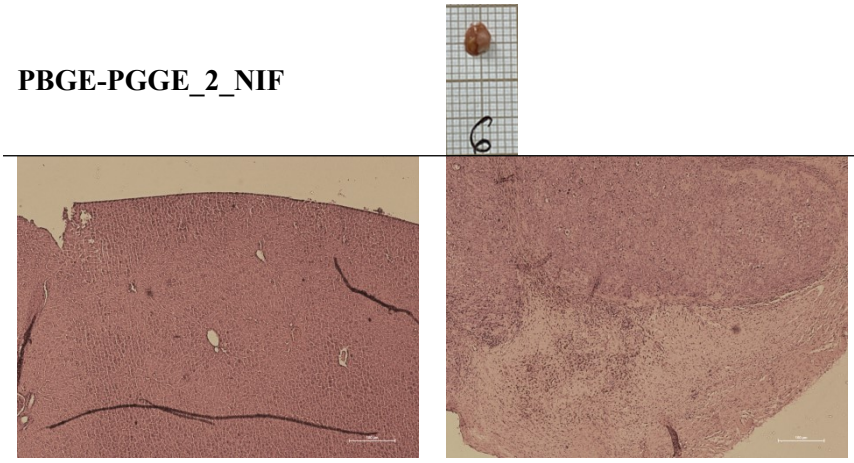

lack of large tumor

liver (6) tumor (6) tumor

Liver (6): Despite extensive macrovesicular steatosis, the liver parenchyma retains its lobular architecture. Almost all hepatocytes contain a single large lipid vacuole, which pushes the nucleus to the edge of the cell. There are no significant inflammatory infiltrates or signs of fibrosis in the liver parenchyma.
Tumor (6): A malignant tumor with a biphasic structure consisting of an epithelioid component (with cells with large, eosinophilic nuclei) and a spindle cell (sarcomatoid) component.

PBGE-PGGE_1_NIF_gel

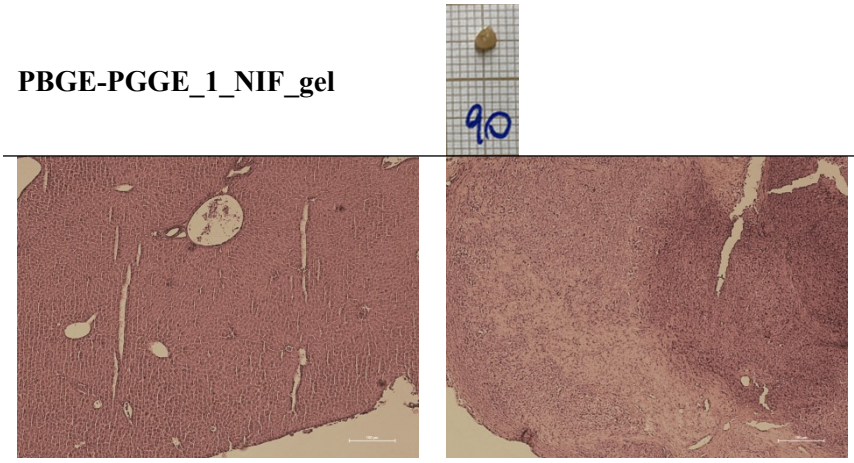

lack of large tumor

liver (90) tumor (90) tumor

Liver (90): The liver parenchyma has fully preserved, normal lobular architecture. The hepatocytes are arranged in regular single-cell plaques that radiate around the central veins. The hepatic cells are polygonal with abundant eosinophilic cytoplasm and a nucleus located in the center of the cell. Unaltered sinusoidal vessels can be seen between the trabeculae. The portal spaces (triads) appear normal.

Tumor (90): Mesenchymal neoplasm composed of pleomorphic spindle cells arranged in irregular fascicles.

PBGE-PGGE_2_NIF_gel

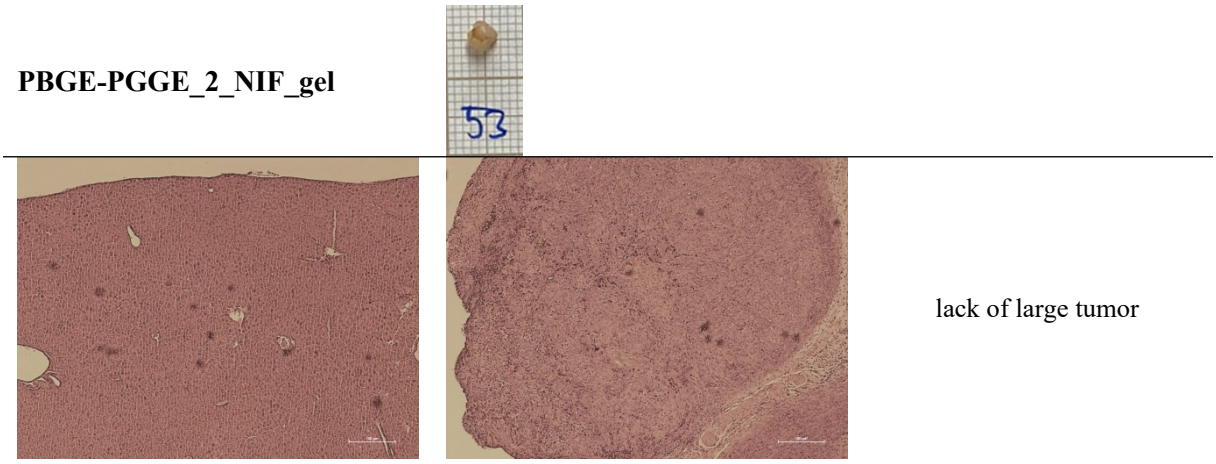

liver (53) tumor (53) tumor

Liver (53): Liver parenchyma with preserved lobular architecture, but evidence of damage present. There are numerous diffuse microfocal lesions within the lobules, characterized by necrosis of single hepatocytes or small groups of hepatocytes. Small clusters of inflammatory cells are visible at the sites of damage, but the infiltration is relatively sparse.
Tumor (53): Excessive cellular and nuclear pleomorphism and an anaplastic appearance of cells with giant nucleoli.

Nifuratel

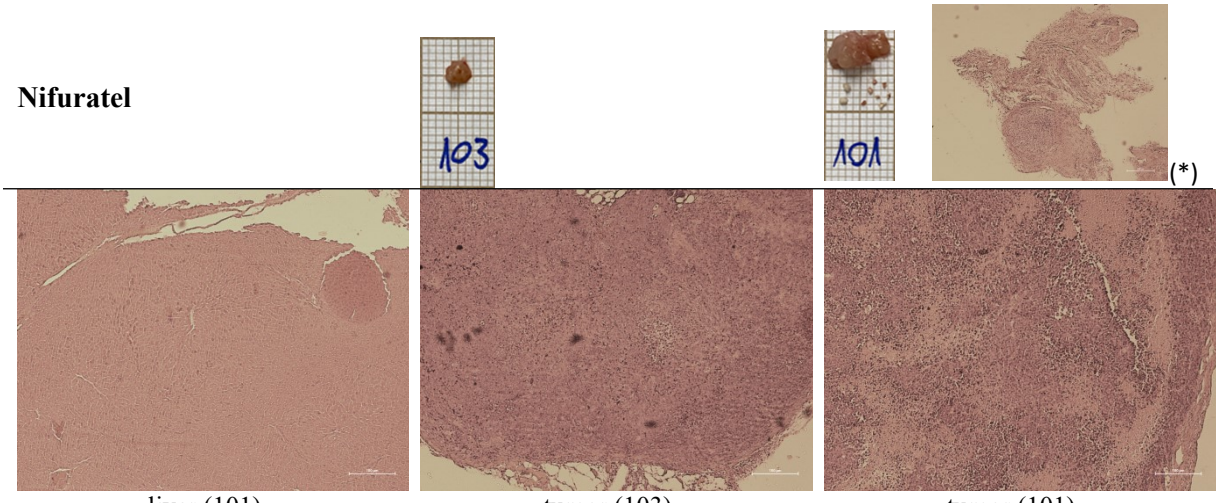

liver (101) tumor (103) tumor (101)

Liver (101): The architecture of the liver is focally disturbed by the presence of a large, well-defined hyperplastic nodule. This nodule is composed of hepatocytes that appear benign and form slightly thickened and irregular plaques. The nodule does not contain any visible portal triads.
Tumor (103): This is a mixed-pattern tumor containing anaplastic cells with giant, eosinophilic nuclei and abundant brown deposits. The tumor infiltrates the adipose tissue.
Tumor (101): A dense, diffuse infiltration of monotonous, medium-sized lymphoid cells with a very high mitotic index and numerous macrophages, creating a 'starry sky' appearance.
Metastasis (*): A tumor with solid, chaotic growth, composed of pleomorphic cells with severe nuclear atypia. The tumor shows no evidence of differentiation in any direction.

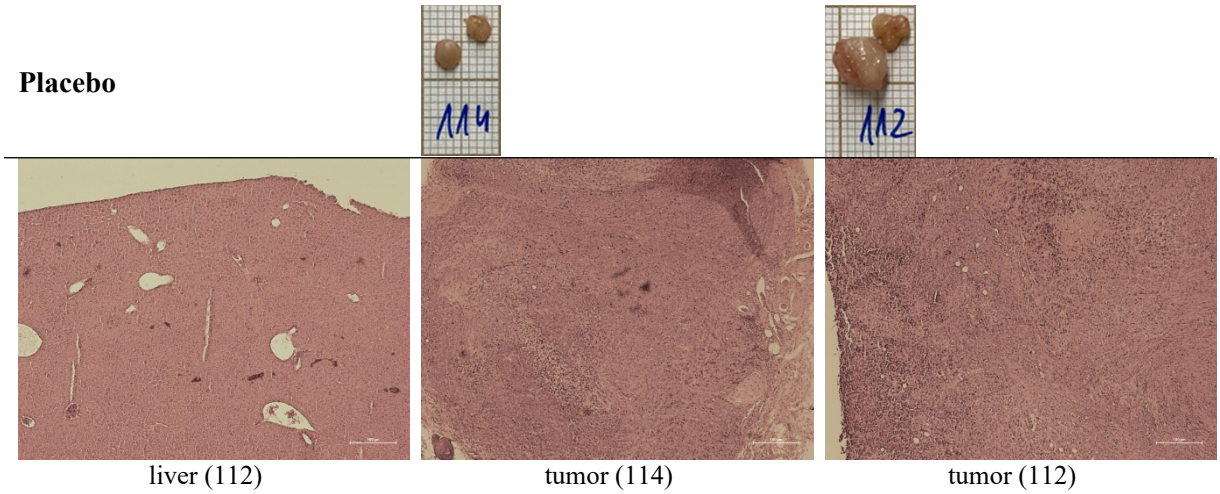

Liver (112): Liver parenchyma with advanced chronic changes. Numerous thin bands of connective tissue (fibrous septa) connect adjacent portal spaces and central veins, resulting in bridging fibrosis and distortion of the normal architecture. A chronic inflammatory infiltrate is visible within the septa.
Tumor (114): A poorly differentiated solid tumor composed of pleomorphic epithelioid and spindle cells, many of which have large, eosinophilic nucleoli.
Tumor (112): A tumor composed of anaplastic epithelioid cells with giant, eosinophilic nucleoli. There are numerous brown deposits within the tumor tissue.

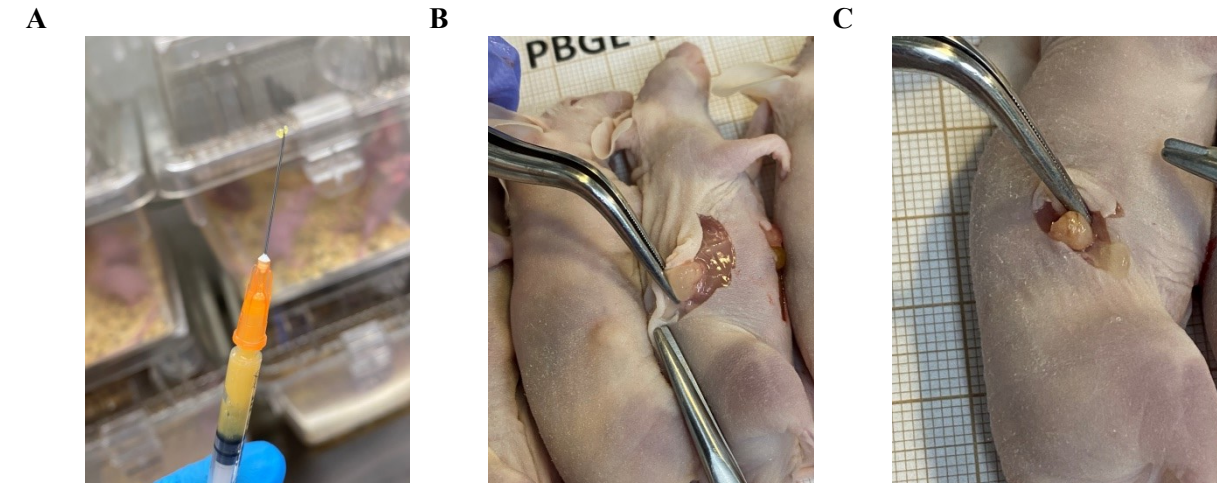

Figure S24. Photos of the yellow nifuratel gel before injection (A) and of the polymer pads with released drug, both without (B) and with (C) tumor.